Towards A Robust Reach Onset Decoder for Electrocorticography-based BCI's

APPROVED BY

SUPERVISING COMMITTEE:

Ashish Desphande, Supervisor

Zoltan Nadasdy

Towards A Robust Reach Onset Decoder for Electrocorticography-based BCI's

by

Patrick Joseph Marino,

THESIS

Presented to the Faculty of the Graduate School of

The University of Texas at Austin

in Partial Fulfillment

of the Requirements

for the Degree of

MASTER OF SCIENCE IN ENGINEERING

THE UNIVERSITY OF TEXAS AT AUSTIN

May 2018

Dedicated to the patient who made this work possible.

Acknowledgments

I wish to thank my family for their continued support, Dr. Deshpande for enouraging me to pursue my interests, Dr. Nadasdy for his advice, and Dr. Buchanan for the opportunity to work with his patients.

Towards A Robust Reach Onset Decoder for Electrocorticography-based BCI's

Patrick Joseph Marino, M.S.E.
The University of Texas at Austin, 2018

Supervisor: Ashish Desphande

Over the past 15 years, rapid research progress has led to electrocorticography (ECoG) emerging as a promising recording modality for brain-computer interface driven upper-limb neuroprosthetics. For example, it has recently been shown that ECoG arrays are suitable for chronic implantation [22] and that the recorded signals contain sufficient information for continuous decoding of three-dimensional hand position [13] [15]. While these advances have demonstrated the feasibility of using ECoG to control upper-limb neuroprosthetic devices, further work is needed to make these devices accurate, safe, and reliable.

State-of-the-art position decoders predict hand position from ECoG signals using various forms of regression, and prediction errors from these models often cause the decoder to detect motion even when the user is at rest [13] [15]. If these algorithms were used for online control of a robot,

this unwanted motion could cause damaging collisions with nearby objects or people. A potential approach to solving this problem is to create another type of decoder which prevents motion until the user's desire to begin a reach is detected. Such a decoder is known as a "reach onset decoder," and works by classifying each moment in time as either "reach onset" or "not reach onset." Although these classifiers are considered by some to be essential for the safe operation of any BCI-driven manipulator [9], high-performance reach onset decoders have only been designed for single-cell BCI's [9]. Such decoders for ECoG BCI's are still in the rudimentary stages of development.

Because the primary purpose of a reach onset decoder is to prevent unintended motion, the most important performance metric for such an algorithm is the false positive rate. This metric quantifies the rate at which the decoder incorrectly detects a reach, thereby allowing for the unintended motion the decoder was designed to prevent. Care must be taken when lowering this rate, however, since there is a tradeoff between the false and true positive rates for any classification algorithm. Thus, the proper strategy when designing a reach onset decoder is to lower the false positive rate to an acceptable level before increasing the sensitivity.

There are several features of ECoG signals that could prove useful for decoding reach onset. In particular, previous studies have identified characteristic patterns of neural activity that emerge when many trials of ECoG data recorded during cued motor movements are averaged together [14] [7] [6]. Known as event related synchronization or desynchronization, these patterns

consist of changes in signal power in certain frequency bands during an event (bodily motion, in this case). However, whether these patterns can be detected during naturalistic reaches on a single-trial basis remains an open question.

To determine whether this is the case, we had a subject implanted with a sensorimotor ECoG grid repeat the naturalistic, sequential reaching and grasping task from [13]. In this task, the subject moves blocks around a table with no rest in between movements. Thus, the reaches involved are self-paced, subtle, and are not separated by resting periods, just as the most difficult reaches to detect in activities of daily living would be. We first show that similar patterns of ERD and ERS to those found in previous studies exist around the onset of reaches in our task. Next, we use these features as inputs to a k-nearest neighbors classifier and decode reach onset with a false positive rate of 1.3% and a sensitivity of 44%. In addition to having functional significance for ECoG BCI's, these results also have potential implications for EEG and single-cell BCI's, since correlates of event related synchronization and desynchronization can be found with these modalities.

Table of Contents

List of Tables

List of Figures

Chapter 1

Introduction

With the possibility of providing a direct communication link between a brain and a computer, Brain Computer Interfaces (BCI's) offer a promising avenue for creating naturalistic neural prosthetics. In principle, a paralyzed individual using a BCI could control a robotic arm with similar ease and dexterity to a healthy person controlling his or her own arm. But in spite of the immense research effort and resources devoted to its development over the last 15 years, such a naturalistic neuroprosthetic arm is still far from being clinically available.

Many of the bottlenecks that prevent the widespread availability of a naturalistic BCI-driven arm arise from the challenges associated with accurately recording the relevant neural activity. In general, there is a tradeoff between the invasiveness of a recording modality and the achievable spectral and temporal resolution in its signal. Thus, improving the accuracy of extracted control signals often comes at a high cost, both financially and in terms of safety and comfort.

An illustrative example of this tradeoff is the microelectrode array, which is the most invasive recording modality (Figure 1.1). While this array is

capable of recording the spiking of individual neurons and local field potentials, it requires a surgical implantion in which the array penetrates the cortex. Patients implanted with these arrays have been able to control a robotic arm with reasonable dexterity, but the arrays suffer from stability and safety issues [5]. The electrodes cause glial scarring around the implant site, which degrades the signals over time, and the transcranial headstage carries a risk of infection [19]. Furthermore, the electrodes shift in position over time, so that different (and usually fewer) neurons are recorded over time.

The least invasive modality, scalp EEG (Figure 1.1), does not require surgery and poses few, if any, safety issues. However, since the electrodes are placed on the scalp, 2-3 centimeters away from the cortex, EEG inherently has low spatial and spectral resolution and is only capable of recording sycnhronized activity from large patches of cortex. Decoding accurate, continuous motions from this type of data has proven to be difficult. Bradberry *et al.* achieved correlation coefficients between decoded and actual 3D wrist position of 0.19 - 0.38 [2], which are far from sufficient to achieve dexterous control of a robotic arm.

With ECoG (Figure 1.1), which is surgically implanted but rests on the surface of the cortex, activity is recorded from finer cortical patches than EEG, offering something of a compromise between scalp EEG and microelectrode arrays. Because ECoG grids rest on the surface of the cortex rather than penetrating it, they do not cause permanent damage of the brain tissue and are not susceptible to glial scarring. Because the grids record from large

groups of neurons, the recorded signals are robust to small positional shifts of the electrodes. These characteristics make ECoG grids safer and more stable than microelectrode arrays. Furthermore, since the grids are implanted on the cortex rather than placed on the scalp, they have much higher spectral and spatial resolution than EEG, allowing for substantially more accurate signal decoding. This may allow ECoG to serve as a testbed for correlation of microelectrode and EEG signals, leading to higher decoding performance for EEG-based BCI's. Perhaps the biggest advantage of ECoG, however, is that its implantation can be part of a clinical treatment plan for patients with intractable epilipsy. Thus, human subjects with these implants are often available. For these reasons, ECoG has become a promising BCI recording modality over the last decade.

To date, several groups have tried to decode continuous 3D hand position with ECoG in both human subjects and non-human primates and have had reasonable success[13] [15]. Hand position has been decoded for several types of tasks, including delayed reaches, sequential reaches, and continuous arm motion, and correlation coefficients between actual and predicted positions in these studies range from 0.4 to about 0.8 [13] [15]. While the magnitudes of these coefficients show that positional information is encoded in the signals, the positional error is at times as high as 10 centimeters [13] [15], so there is still much room for improvement.

In addition to producing inaccurate trajectories, the positional errors in the predictions from a decoder can also cause motion to be predicted when

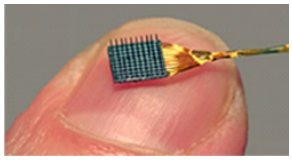

(a) Microelectrode Array [3]

(b) EEG [11]

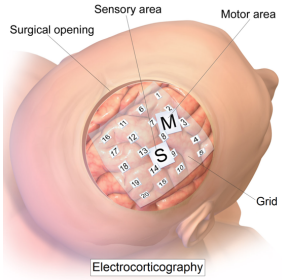

(c) ECoG [20]

Figure 1.1: Three BCI recording modalities: (a) the Utah Array, a popular microelectrode array, (b) scalp EEG, (c) an ECoG grid. The Utah Array is surgically implanted and records the activity of individual neurons as well as local field potentials. Scalp EEG in non-invasive and records large-scale neural oscillations which have been low-pass filtered by the scalp. ECoG is surgically implanted and records neural oscillations with much higher resolution than scalp EEG.

the user is at rest. If the decoder were used to control a manipulator, these unintended motion predictions could result in damaging collisions with nearby people or objects. Since prediction errors are inherent to the models used to decode position, determining when the user desires to move, and, more importantly, when he or she does not, is crucial for the safe and reliable operation of a BCI-driven manipulator.

One approach to solving this problem is to create another decoder, known as a "reach onset decoder," which determines when the user desires to begin a reaching motion. Such a decoder would work by classifying each time point in the operation of a BCI as either "reach onset" or "not reach onset." Since the primary purpose of the decoder is to prevent unwanted motion, the

most important performance metric for such an algorithm is the false positive rate. This metric quantifies the rate at which the decoder incorrectly detects a reach, thereby allowing for the unintended motion the decoder was designed to prevent. Care must be taken when lowering this rate, however, since there is a tradeoff between the false and true positive rates for any classification algorithm. Thus, the proper strategy when designing a reach onset decoder is to lower the false positive rate to an acceptable level before increasing the sensitivity.

Effective reach onset decoders for microelectrode-based BCI's have already been successfully developed using relatively simple methods. Hwang and Andersen, for example, created a threshold-based onset decoder using local field potentials from the parietal area of a rhesus monkey [9]. Using the local field potentials recorded at only a single microelectrode, the decoder detected reach onset with high accuracy. It worked by summing the derivatives of the power in two different frequency bands at each time step, then scaling the sum and comparing it to a threshold value. Because of the strong correlation between parietal local field potentials and reach onset, designing an onset decoder with such data is straighforward.

Identifying reach onset is more challenging with ECoG because of the qualitative differences between signals recorded with microelectrode arrays and those recorded with ECoG electrodes. Microelectrode arrays can record either the spiking activity of individual neurons or local field potentials, and although neither are well understood in general, several studies have shown

that, for certain specific subpopulations of neurons, these measures are closely correlated with kinematic parameters. For example, the classic "cosine tuning" result showed that the firing rates of some motor neurons are proportional to the dot product of the neuron's preferred direction and the velocity of the hand [8]. When such straighforward relationships exist, simple algorithms are sufficient for predicting behavior. The relationship between the neural activity recorded by ECoG and motor parameters is not as clear. Since an ECoG electrode records the activity of hundreds of thousands of neurons, it is not possible to discern individual firing rates. Instead, we take advantage of the fact that large groups of neurons tend to transiently synchronize their firing activity, producing increased power at the frequency at which this firing occurs. Thus, when such a power increase occurs, there is said to be "synchronization" in that freqeuncy band, and when the power decreases, "desynchronization." Although no obvious relationships between neuronal synchronization and arm position have been discovered, positional decoders for ECoG signals such as those discussed above have been successfully developed by fitting measures of neural power at several frequencies and time lags to arm motion with various regression algorithms [15] [13].

Sychronization and dysynchronization patterns have, however, been related to the *onset* of a few bodily motions [14] [7] [6]. By time-averaging many trials of noisy neural activity around movement onset, several studies have identified specific patterns of synchronization and desynchronization over the sensorimotor cortex that accompany movement onset. Since these patterns

occur around an event (movement onset, in this case), they are termed, "event-related" synchronization or desynchronization (ERS or ERD, respectively, for short). In addition to averaging many trials together to remove noise from the signals, these studies took futher steps to make the patterns discernable. Subjects were asked to make motions designed to elicit a large neural response over the motor areas due to their high homuncular representation, such as tongue protrusion, foot flexion, or palmar grasp. They were also asked to rest for several seconds in between motions. The neural activity during motion was then compared to the quiter neural activity during rest, which was taken as a baseline.

To complete activities of daily living, however, a BCI-driven manipulator would need to be capable of recognizing desired movement onset when the associated neural signatures are more subtle. Many tasks consist of several small, sequential steps that are completed with no resting periods between succesive movements. For example, one can imagine washing a dirty plate. Movements in this task, such as turning on the faucet, pouring soap onto the plate, and picking up a sponge require only small forces and motions and are not separated by appreciable amounts of rest. Even if neural data were time-averaged around such movements, would they be accompanied by similar ERD and ERS patterns as described in [14] [7] and [6]? And, given that such data is characterstically noisy, is there any hope of accurately identifying the onset of each movement on a single-trial basis?

In this study, we set out to answer these questions. We had a subject

implanted with a sensorimotor ECoG array for the treatment of intractable epilipsy complete a task borrowed from Nakanishi, *et al.*, in which the subject continously moves blocks around on a table in front of him or her [13]. In this task, there are no rest periods in between successive motions, and the reaches are all small and self-paced, so they are representative of the most difficult reaches to detect in naturalistic situations. We time-averaged the ECoG data around reach onset and showed that ERD and ERS patterns similar to those described in [14] [7] and [6] do exist around such motions. With this knowledge, we designed a reach onset decoder based on a k-nearest neighbor classifier to take advantage of these patterns, and we achieved high decoding accuracy for movement onset using relatively few features. These findings have several implications. First, they indicate that ERD and ERS values contain sufficient information to decode reach onset, even for subtle reaches. Second, they suggest that k-nearest neighbor classifiers may be suitable for handling the high trial-to-trial variablility in ECoG data. Finally, since ERD and ERS or their correlates can be observed in EEG and single-cell BCI's, they could potentially be used to improve the performance of decoders for those modalities.

Chapter 2

Methods

2.1 Experimental Subject

This study consisted of one patient with intractable epilepsy who underwent clinical subdural ECoG monitoring for seizure localization. The study was performed at Dell Seton Medical Center at the University of Texas at Austin (Austin, TX). The study was approved by the Seton IRB, and the subject provided informed consent. Information about the patient and the implanted electrodes can be found in Table 2.1. The implant locations are pictured in Figures 2.1 and 2.2. As can be seen in the figures, the patient had bilateral grids, primarily located on the right hemisphere, with a large grid located over the right sensorimotor region. A total of 124 electrodes were implanted.

The patient was unusually drowsy for three days after the implant. On the fourth day after the implant, a headache and continued drowsiness prompted a CT scan, which revealed a fluid buildup in the left frontal region between the skull and dura. The fluid was surgically drained in the afternoon of the fourth day after implant, and the ECoG grids were left in place. Shifting of the grids relative to the implant location appeared to be minimal. Six

days after the implant, the subject recovered and completed an experimental trial. However, vision in one eye was blurry, so a patch was worn over that eye. Frequent seizures prevented data collection on the seventh day after the implant, but another experimental trial was completed on the eighth day. On that day, vision in both eyes was normal, so no eye patch was worn.

Table 2.1: Patient Information

Sex	Handedness	Age	Cognition	Hand Used	Number of Electrodes	Electrode Location
F	Right	33	Normal	Left	124	Left Frontal (1x6), Right Frontal (4x5), Medio-Temporal (1x6), Parietal (1,6), Occipital (1x6), Parieto-Temporal (1x6), Right Temporal (4x8), Right Sensorimotor (4x8), AT (2x6)

2.2 Task

The subject performed a repetitive, naturalistic reaching and grasping task as in [13]. In this task, three wooden cubes with a 1 inch side length were placed on a table in front of the patient, arranged at three of the corners of a 25x25 centimeter square, leaving one of the corners empty (Figure 2.3).

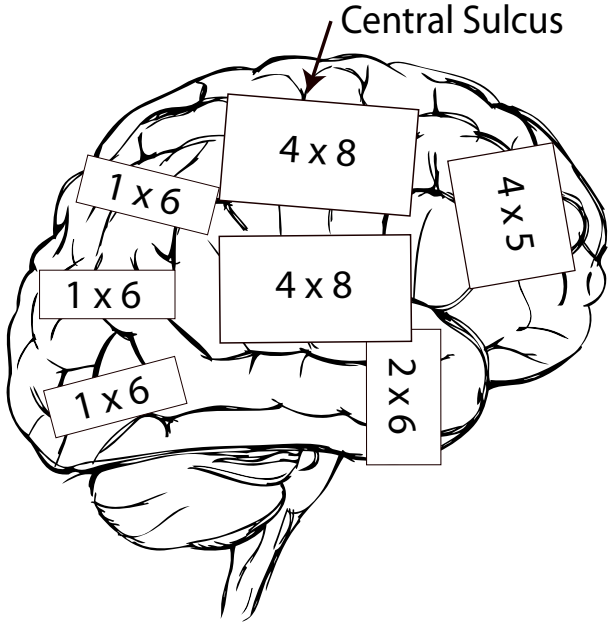

Figure 2.1: Right hemisphere electrode placement. Large (4x8) grids were implanted over sensorimotor and temporal regions. Smaller grids and strips were implanted in many areas, notably over the parietal and occiptal lobes.

After seeing a visual cue that indicated the neural and motion data were being collected and had been synchronized, the patient was instructed by the experimenter to begin motion. The patient then began a series of self-paced reaches that lasted for the duration of the experimental session. For each reach, the patient picked up one of the blocks adjacent to the empty corner of the square and moved it to that corner, leaving a new empty corner behind. This was repeated for the entire session, always moving the blocks in a counter-clockwise direction. Since the ECoG grids were primarily placed in the right hemisphere, the subject was instructed to move the blocks using the left hand.

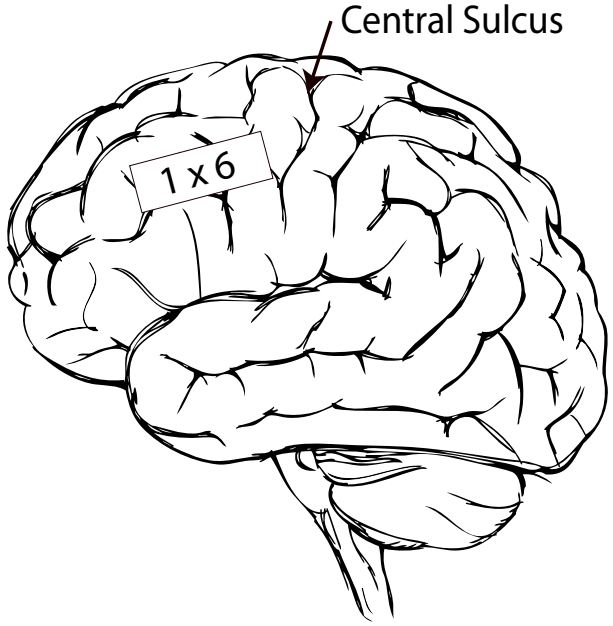

Figure 2.2: Left hemisphere electrode placement. Only one strip was implanted in the left hemisphere. It was placed over the left frontal region.

Single sessions lasted an average of 2 minutes and 30 seconds, and consisted of uninterrupted picking and placing. Five sessions were conducted on each day of the experiment, so that the total amount of data collected was about 15 minutes. Each day of data was analyzed seperately.

2.3 ECoG Signals and Motion Recordings

The ECoG signals were recorded on a 128-channel digital EEG system (Neuralynx ATLAS; Neuralynx, Bozeman, MT) and sampled at 2000 Hz. All electrodes were referenced to an inverted, subdural reference electrode, then

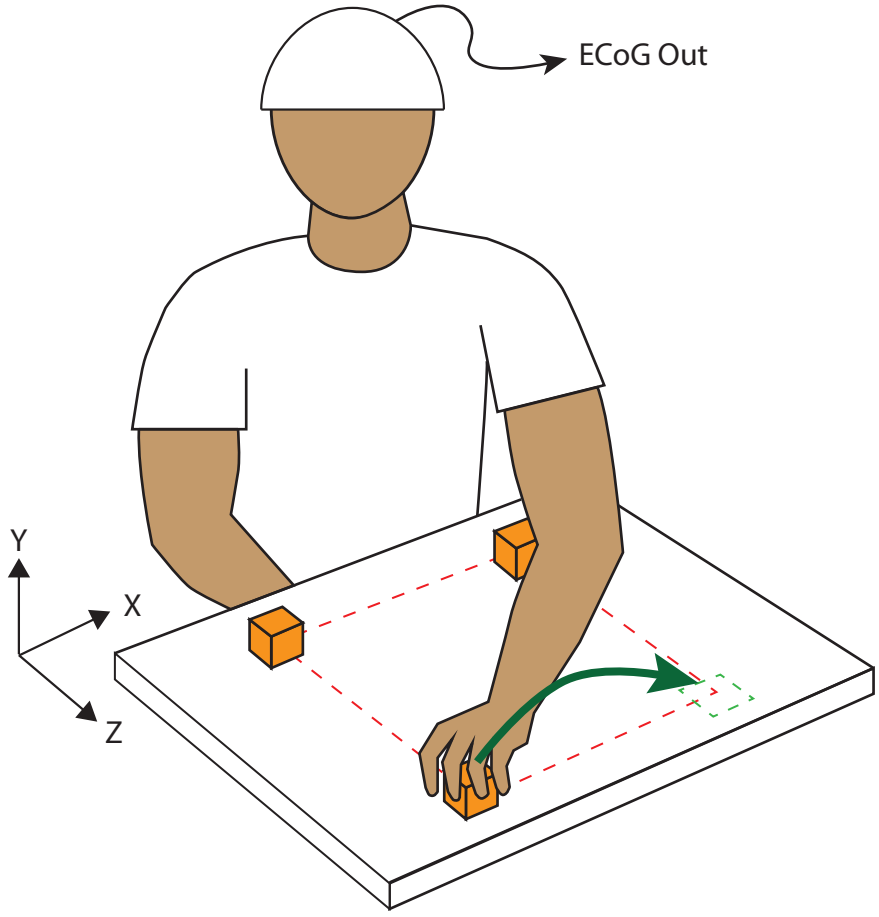

Figure 2.3: In our experimental setup, the patient's bed was elevated so that the patient sat as upright as possible. The bedside table was then positioned over the patient's lap, so that the entire surface of the table was within the patient's reach. A mat with a 25x25 cm square marked on it was placed on the the table, and the three cubes were placed at three vertices of the square. After receiving the go cue, the patient moved one block at a time to the empty vertex of the square, always in a counter-clockwise direction. This was repeated without rest for two minutes and thirty seconds on each trial.

re-referenced to the quietest electrode in the 124 channel array. Electrical noise was filtered out at 60, 120, and 180 Hz using 3rd order, zero-phase lag butterworth filters with a width of 4 Hz. ECoG signals were then common average referenced.

3D arm motions were recorded using an infrared LED motion capture system (Phasespace X2; Phasespace, San Leandro, CA). Markers were placed on the patient's left shoulder, elbow, wrist, hand, and chest to monitor any motion of the body. Position data from the markers was sampled at 480 Hz. The onset of each reach was located in the motion data by visual inspection - onsets coincided with peaks or troughs in the data when the wrist was located at the vertices of the square.

Reaches were always carried out in the same sequence: first, the top right block was moved left to the empty top right corner (the "top" half of the square was the one furthest from the patient). Next, the patient reached to the back right block and moved it forward to the newly vacated top right corner. Next, the patient reached to the back left block and moved it right to the newly vacated back right corner, and so forth. In this way, the data could be seperated into eight distinct reach types: left, right, forward, back, forward left, forward right, back left, and back right. It is worth nothing that the resulting reaches were not symmetric, as in a classic 8-target center-out task. For example, right reaches always occured along the side of the square closest to the patient, whereas left reaches occured along the side of the square farthest from the patient.

The ECoG and motion capture signals were synchronized using an external laptop and a Cedrus StimTracker (Cedrus StimTracker; Cedrus, San Pedro, CA). Synchronization pulses from the external laptop were sent at regular intervals for the duration of the experiment, so that in addition to synchronizing the starts of each data stream, clock drift could be corrected.

2.4 Quantification of ERD/ERS

In order to measure event related synchronization or desynchronization (ERS or ERD) at reach onset, the procedure used by Pfurtscheller *et al.* was applied [14]. In our case, each trial consisted of a 1 second window centered around a reach onset. Since the sampling frequency was 2000 Hz, each trial consisted of 2000 samples.

The ECoG signals from each trial were bandpass filtered into overlapping bands that were 10 Hz wide with 5 Hz of overlap, resulting in bands of 1-10 Hz, 5-15 Hz, 10-20 Hz, and so forth, up until 90-100 Hz. Again, third order, zero phase lag butterworth filters were used. Next, for each electrode, the time-varying power in each frequency band was calculated as

$$y_{ij} \;=\; (x_{ij} - \bar{x_j})^2 \tag{2.1}$$

in which y_{ij} is the power of the jth sample of the ith trial, x_{ij} is the voltage of the jth sample of the ith trial, and $\bar{x_j}$ is the mean voltage for the jth sample

averaged over all trials.

Then the average power for each sample over all trials was calculated:

$$A_j = \frac{1}{N-1} \sum_{i=1}^{i=N} y_{ij} \tag{2.2}$$

where N is the number of trials. Then A_j was averaged over all samples to get the baseline power, R :

$$R = \frac{1}{2000} \sum_{i=1}^{i=2000} A_j \tag{2.3}$$

Finally, the ERD or ERS was calculated as a percentage change from baseline of the average power:

$$ERD_j = \frac{A_j - R}{R} \times 100\% \tag{2.4}$$

To establish the statistical significance of ERD/ERS values, the bootstrapping method from [14] was applied. Only values that were significant with 99 % confidence were considered.

2.5 Modulation Index

We wished to quantify the degree to which each electrode exhibited beta ERD and gamma ERS during reach onset. This measure served two purposes. First, it allowed us to identify those electrodes which were highly modulated by movement onset. Second, these values were be used to create a spatial map of electrode modulation during onset, enabling us to identify key neuroanotomical areas for controlling reach onset.

Thus, we defined the "Modulation Index" as the difference between the maximum gamma ERS value and minimum beta ERD value at each electrode during reach onset:

$$\text{Modulation Index } = \max(\text{gamma ERS}) - \min(\text{beta ERD}) \tag{2.5}$$

2.6 k-Nearest Neighbors Classifier

Once it was established that statistically signifcant beta ERD and gamma ERS accompanied reach onset in select sensorimotor electrodes, we decoded reach onset using these features as inputs to a classifier. We created our target dataset by labeling each point in the motion data as "movement onset" or "not movement onset." Movement onset periods were defined as +/- 200 ms time windows centered around the reach onset times. All other time points were lableled not movement onset.

In order to create the input data for our classifier, we sampled beta

ERD and gamma ERS values at the two sensorimotor electrodes with the highest modulation indices. For each time point in the target dataset, our input consisted of the previous 500 ms of ERD and ERS values, sampled once every 50 ms, for a total of 40 predictor variables (ten samples of beta and ten samples of gamma at each of two electrodes). Finally, the input data was shuffled before training the classifier.

After creating our input and target datasets, we selected our classification algorithm by running a preliminary analysis using MATLAB's Classification Learner Toolbox (Mathworks, Inc.; Natick, MA). The set of alrorithms tested included decision trees, linear discriminant classifiers, logistic, regression, support vector machines, and nearest neighbor classifiers [10]. Of these algorithms, we found that nearerst neighbor classifiers performed the best on our dataset.

The k-nearest neighbors classifier [10] works by estimating the conditional probability that an observation belongs to a class j, given its predictor values, x_o. It estimates this probability, $P(Y = j|X = x_o)$, as the fraction of the k nearest points to x_o in the training data that belong to class j, asssigning x_o to the class for which that fraction is the highest.

Thus, for a given test point x_o, the estimated conditional probability of the point belonging to class j is

$$P(Y = j|X = X_o) \ = \frac{1}{k} \sum_{i=1} I(y_i = j) \tag{2.6}$$

and this calculation is repeated for each class. The classifier then assigns to the test point the class with the highest conditional probability.

In order to assess and optimize the performance of our classifier, we created an approach customized for our application. First, although the training set was shuffled, we tested the classifier on unshuffled data to simulate natural conditions. Our most important criterion was a low false positive rate, calculated in the usual way. Our next criterion was the true positive rate, but we calculated this in a way that reflected the nature of our application: each reach onset period was considered a single positive event, even though each of these periods lasted several time steps. If our classifier labeled one or more of those time steps positive, we considered the label a true positive. If none of the time steps during the reach onset period were labeled onset, we considered the label a false negative. This is appropriate, since in clinical deployment, a reach onset decoder would only need to detect reach once each time the user desired to make a reach. The results of our classification were validated with 5-fold cross validation.

Chapter 3

Results

3.1 ERD and ERS Around Reach Onset

Event related synchronization in the gamma band and desynchronization in the alpha and beta bands were observed around reach onset on both days of recording. The gamma synchronization began at reach onset and lasted for about 300 ms, taking place over a frequency range of 65-100 Hz. The alpha and beta desychronization began about 250 ms prior to reach onset and lasted for approximately 400 ms, occuring over the range 10-40 Hz. A short beta rebound was observed about 250 ms after reach onset. Finally, there was also significant movement related activity in the delta band (about 5 Hz). Here, desynchronization began about 350 ms before reach onset, with synchronization occuring about 50 ms after onset.

In Figure 3.1, we compare the durations of the beta ERD and gamma ERS in our task to those reported for palmar pinches separated by resting periods (PSRP) in [14]. In the PSRP task, both beta ERD and gamma ERS last substanially longer than in our task, and the gamma ERS is completely embedded in the beta ERD, unlike in our task.

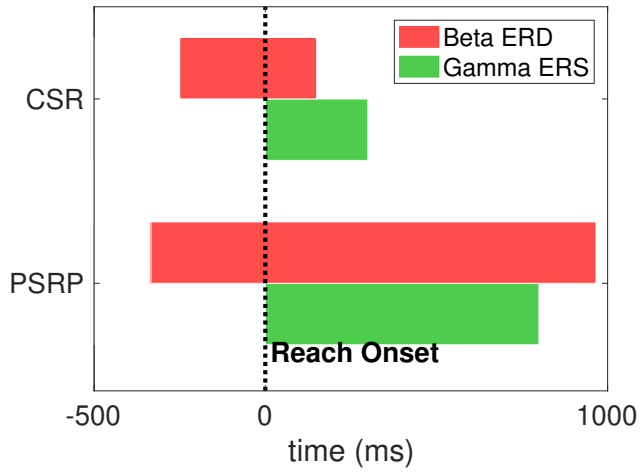

Figure 3.1: A comparison of the duration of beta ERD and gamma ERS observed during our task (CSR, for "Continuous Sequence of Reaches") and during the task from a previous study (PSRP, for "Palmar Pinches Separated By Resting Periods") [14]. For CSR, beta ERD and gamma ERS lasted less time than during PPSRP. Gamma ERS was completely embedded in beta ERD during PPSRP, but not for CSR.

In order to quantify the degree to which beta ERD and gamma ERS occured at a given sensorimotor electrode, we took the difference between the maximum gamma ERS value and minimum beta ERD value observed at each electrode. We call this number the "modulation index" for the electrode. Figure 3.2 presents the modulation indices for each electrode in order to illustrate the spatial distribution of movement-related neural modulation. Modulation was highest along a narrow band near the central sulcus, and it decreased with the radial distance from this location. This pattern was preserved over both days of recording, giving us high confidence that it is representitive of the functional neuroanotomy of the subject. Furthermore, the narrow band

was located near the inferio parietal lobule, just below the intraparietal sulcus, which has been shown to modulate its activity during reaching in several previous studies [9].

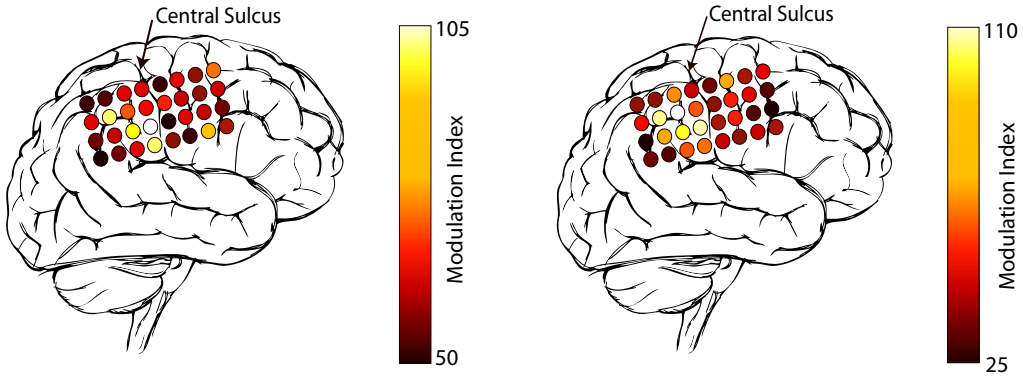

(a) Day 1 (b) Day 2

Figure 3.2: Modulation Indices for Sensorimotor Electrodes: (a) Day 1 and (b) Day 2. The highest modulation values were observed along a narrow band near the central sulcus. As the radial distance from this location increased, the modulation values decreased. This pattern was observed over multiple days of recording.

In order to more precisely charcterize the neural correlates of reach onset, we will now examine the modulated activity at a few exemplary electrodes. We chose electrodes 73 and 83, which had the highest average modulation indices over the two days of recordings. The location of these electrodes is illustrated in Figure 3.3 below. For each electrode, we analyze the modulated activity with two kinds of plots: a two dimensional plot that emphasizes the temporal charateristics of the modulation, and a three dimensional plot that

emphasizes the modulation amplitudes. The ERD and ERS values in the three dimensional plots have been low pass filtered at 5 Hz for smoothness, so that the overall trends in the data are more visible.

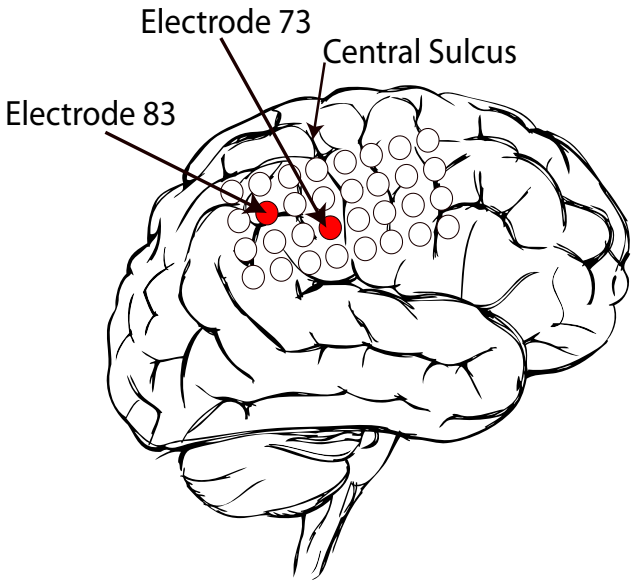

Figure 3.3: Electrodes 73 and 83 were chosen to illustrate the observed patterns of neural modulation. Both of these electrodes were located within the highly modulated band that can be seen in Figure 3.1.

ERD and ERS values around reach onset for electrode 73 are presented in Figures 3.4 and 3.5. We can see that beta desynchronization was most prominent in the 20-30 Hz range, with the power in this band decreasing by about 40% of its mean value before reach onset. A strong beta rebound after reach onset is also visible. Gamma synchronization is strongest at about 95 Hz, increasing 25% relative to its mean value. A large delta peak (40%

increase from mean) can also be seen immediately after reach onset. While these features were preserved across both days of recordings, their magnitudes are higher on Day 2.

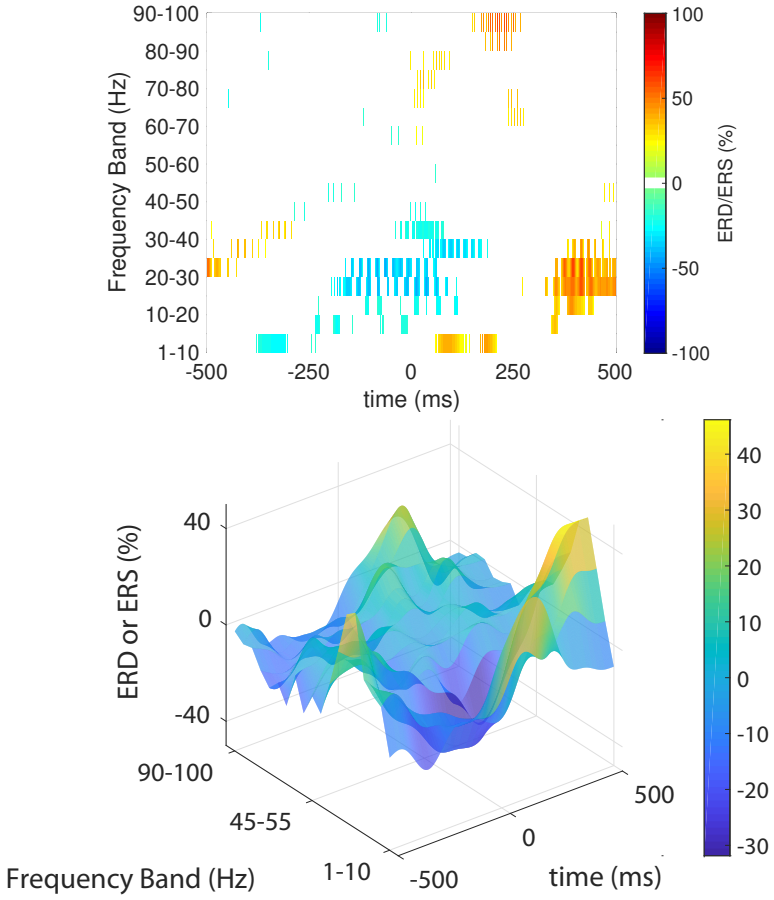

Figure 3.4: ERD and ERS values at electrode 73 during Day 1 of the experiment. Before reach onset, strong beta desynchronization can be seen. After reach onset, gamma synchronization, beta rebound, and delta synchronization are all visible.

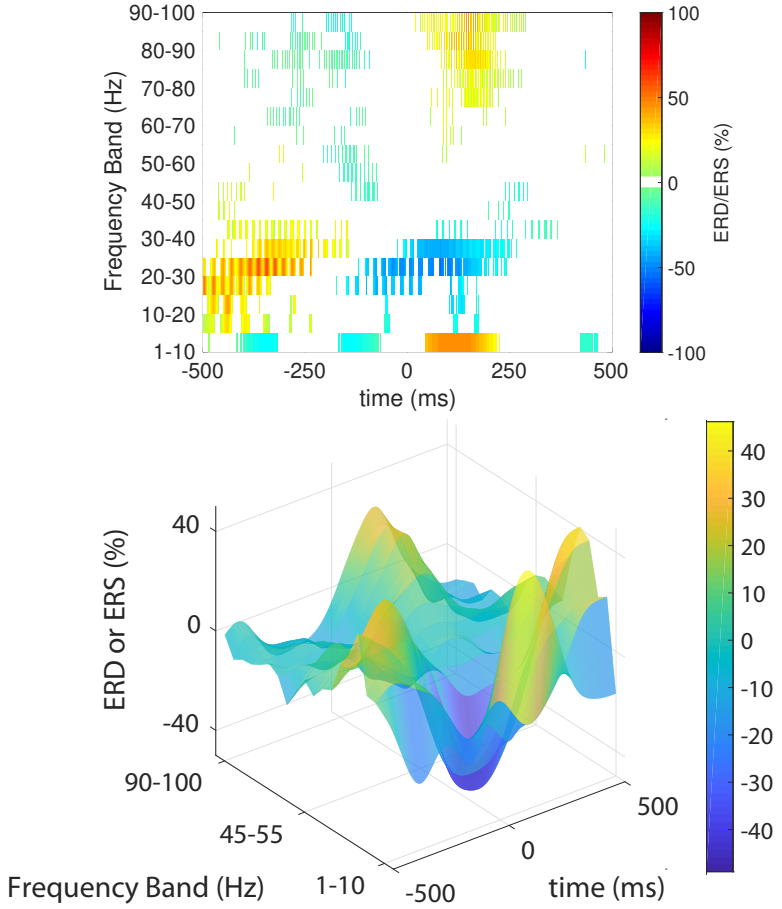

Figure 3.5: ERD and ERS values at electrode 73 during Day 2 of the experiment. Although the overall trends are the same as in Day 1, there are a few notable differences. Gamma synchronization occurs over a broader range, and the magnitudes of modulation are higher for each of the features described for Day 1.

ERD and ERS values around reach onset for electrode 83 are presented in Figures 3.6 and 3.7. Again, we see beta synchronization and rebound in the 20-30 Hz range, gamma synchronization at 95 Hz and delta synchronization at about 5 Hz. The features were higher in magnitude on the second day of

recording at this electrode as well.

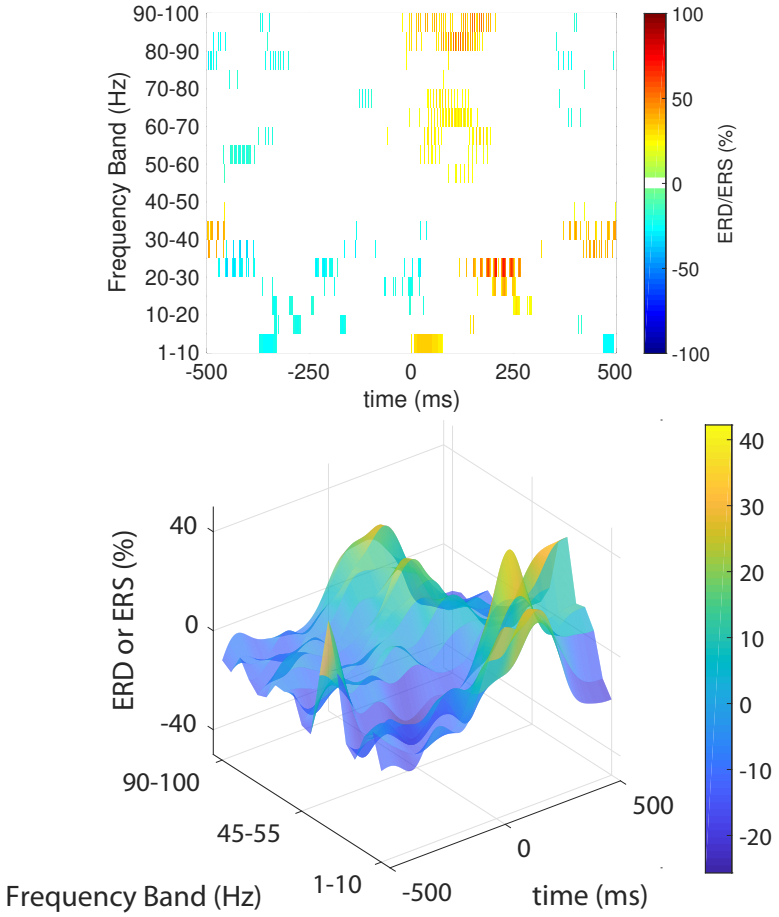

Figure 3.6: ERD and ERS values at electrode 83 during Day 1 of the experiment. As with electrode 73, beta desynchronization takes places prior to reach onset. After reach onset, gamma synchronization, beta rebound, and delta synchronization are exhibited.

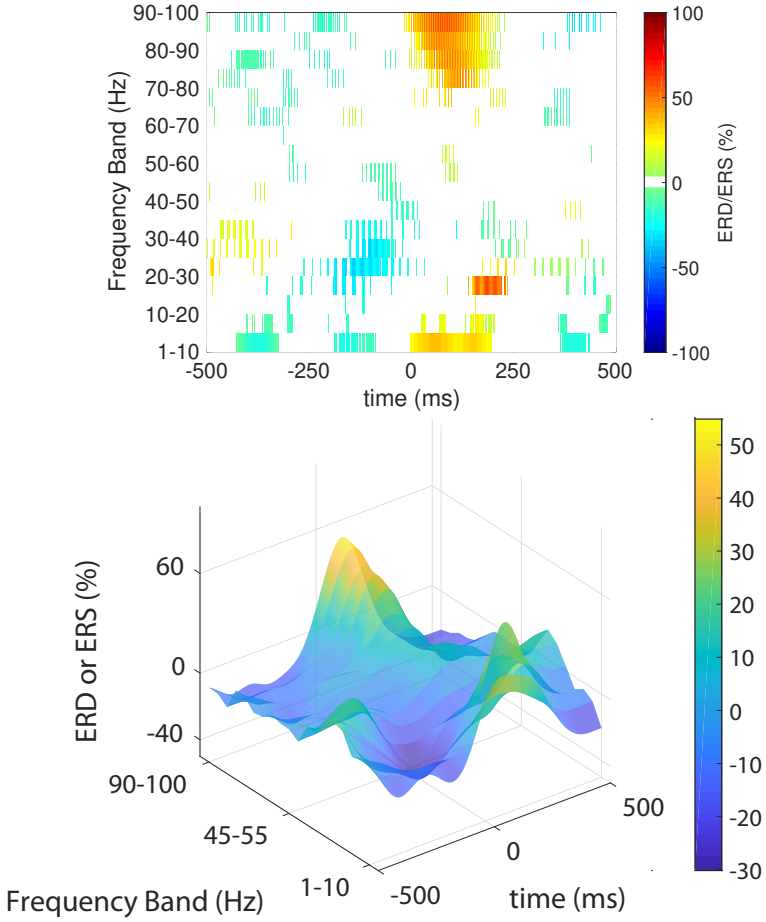

Figure 3.7: ERD and ERS values at electrode 83 during Day 2 of the experiment. The magnitudes of all features are higher during the second day of recording.

3.2 k-NN Reach Onset Decoder

Since the primary role of a reach onset decoder is to prevent unwanted motion, the most important performance metric for our clasifier was the false positive rate. False positive detections indicate that the classifier allowed for

the unintended motion it was designed to prevent. Thus, we first tuned the parameters of our classifier to minimize the false positive rate, then increased the sensitivity as much as possible without exceeding a 2% false positive rate.

Our best performance was achieved by using $k = 5$ nearest neighbors for classification and imposing a cost of 1.5 for false positives and 1 for false negatives. After a 5-fold cross validation, we were able to reduce our false positive rate to 1.3% while still succesfully capturing almost half of all reaches (44%). A confusion matrix showing these results can be seen in Figure 3.8. Although false and true positive rates are one way to evaluate the performance of our classifier, there is no substitute for simulating its performance. In Figure 3.8, we show the output of the classifier for 25 seconds of the task. In the example, we see that out of 21 reaches by the user, we capture 13 of them with only 3 false positive detections.

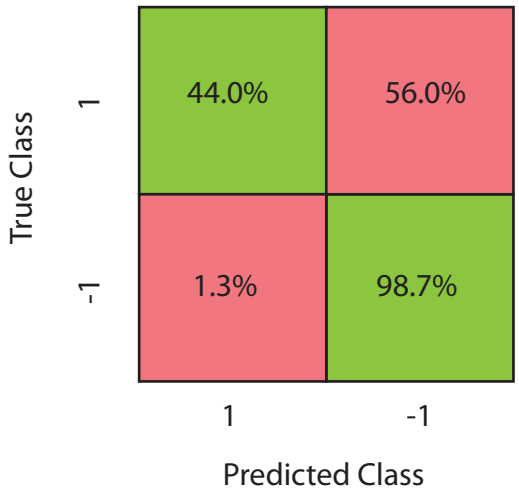

Figure 3.8: Results of 5-fold cross validation. The false positive rate is near 1%, while almost half of all reaches are succesfully detected. This means that when the user did not desire to begin a reach, we correctly determined this almost 99% of the time.

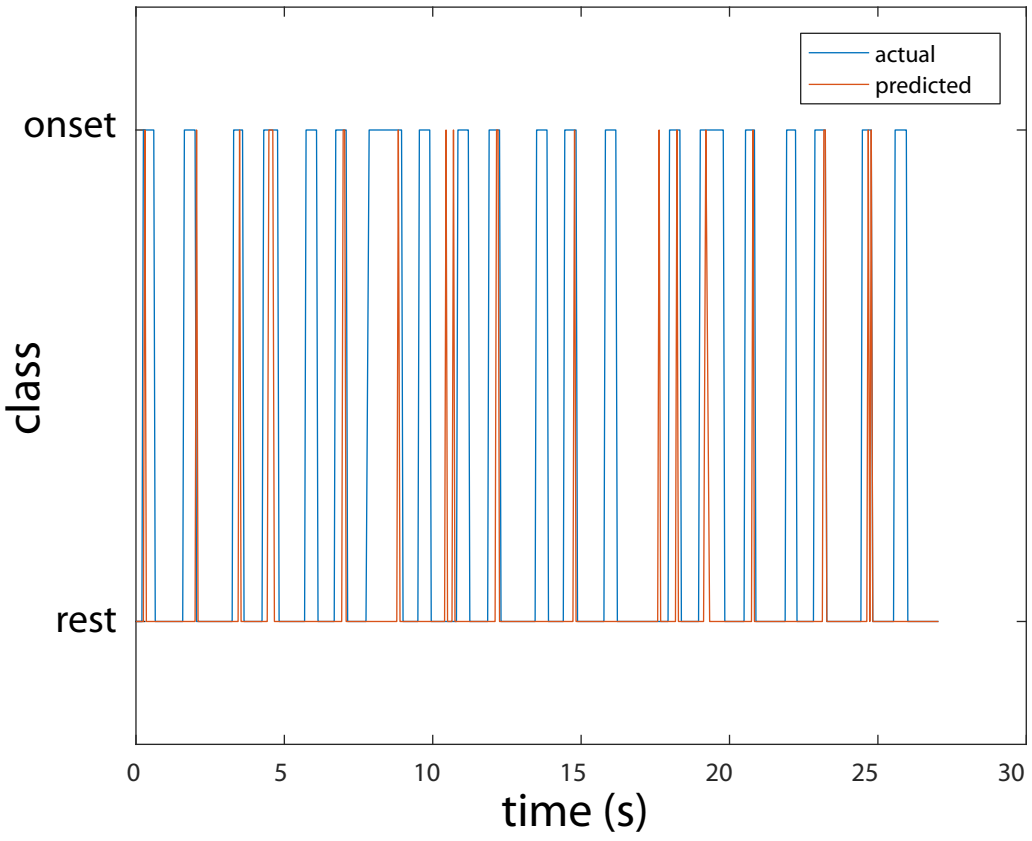

Figure 3.9: Sample performance of our onset decoder. In this example, 13 of 21 reaches are correctly detected, and there are three false positive detections.

Chapter 4

Discussion

4.1 ERD and ERS around Reach Onset

The spatial distribution of sensorimotor electrodes that exhibited beta ERD and gamma ERS around movement onset for our task matched up closely with those observed in [14], [7], and [6]. In all of these studies, there were epicenters of characteristic activity just posterior to the central sulcus on the hemisphere contralateral to the moving arm, and the magnitude of the activitiy decreased with the radial distance from the epicenter. These findings are likely locating the inferio parietal lobule, just below the intraparietal sulcus, which is known to modulate its activity during reaching motions. While the agreement with prior literature increases our confidence in our findings, it may also indicate that macro ECoG contacts have insufficient spatial resolution to differentiate between similar upper limb movements, considering that different upper limb tasks were used in each study. In order to decode subtle arm motions, higher density contacts may be necessary.

The frequency ranges over which movement-related ERD and ERS occured in our subject (65-100 Hz for gamma ERS and 10-40 Hz for beta ERD) were also similar to those observed in previous studies [14], [7], [6]. This would

indicate that similar underlying networks are involved in the execution of these different upper limb motor tasks.

When we compared the duration of the beta ERD and gamma ERS in our task to that during the PSRP task from [14], however, there were a few notable differences. Gamma ERS began at motion onset in both tasks, but lasted much longer in PSRP (250 ms in our task compared to 800 ms in PSRP). Beta ERD began slightly earlier in PSRP than in our task, but lasted more than 3 times as long (400 ms in our task compared to almost 1300 ms in PSRP). Furthermore, while there was an overlap between the two phenomena in our task, gamma ERS was completely embedded in beta ERD in the PSRP task.

In order to interpret these findings, we begin by analyzing the differences between our task and PSRP. In PRSP, subjects made sustained palmar grasps after a resting period during each 6-second trial. In our task, subjects were continually picking and placing blocks without rest, so each trial represents a 1-second window around a reach onset. The same method was applied to both datasets to calculate the ERD and ERS values, and in this method, the baseline power in each frequency band is taken over the entire trial. Since there was a resting period captured in the baseline power calculation in the PSRP task, but not in ours, we would expect that both the duration and magnitude of the spectral phenomena would be lower in our task, which is indeed what we observed.

It has been shown that gamma ERS is correlated to the average firing

rate of neurons in a cortical area [16], and the average firing rate of neurons increases during active computation. In the case of sensorimotor electrodes, underlying computations could reflect the conversion of motor plans into muscle space or the interpretation of tactile feedback from the fingers. Given that gamma ERS occured immediately after reach onset in our task, it could correspond to the muscle contraction at the beginning of a reach or the sensation of grasping a block, whereas in PSRP, it may reflect muscle contraction for a pinch and the sensation of feeling opposing fingertips.

The role of beta activity over motor areas during movement is poorly understood, but some have hypothesized that it is related to planning or readiness. These aspects were likely significantly different in the two tasks. In our task, the data might indicate that in a sequence of reaches, each reach is planned separately before it is executed, or at least that existing plans are updated with the most recent sensory information before execution. In PSRP, this readiness potential might be indicative of the time delay between intention and action.

Recently, we examined a spectrogram of the entire experiment and found that gamma ERS and beta ERD occured on most reaches, but not all of them. This also would have decreased the apparent magnitude and duration of these features in our results. Why these patterns were observed during some reaches but not others could be an exciting future direction for this work. Beta ERD was absent on more reaches than gamma ERS was. Since beta ERD is associated with readiness and planning, one possible explanation for

its absence on some reaches is that the subject sometimes planned multiple reaches ahead. Perhaps beta ERD is only observed in a series of reaches when reach planning is taking place.

Finally, another interesting difference between our results and previous results was the large delta band synchronization that occured just after reach onset. Although this seems to be present in other works, it is not disucssed. Further investigation of this rhythm could be another future direction.

4.2 k-NN Reach Onset Decoder

Our work on decoding reach onset represents a preliminary foray into an area which has not been the subject of much research. While our findings demonstrate that ERD and ERS signals contain sufficient information to decode reach onset above chance levels, further work is needed to improve the performance of the decoder.

In this study, we focused mainly on achieving a low false positive rate, since a reach onset decoder would serve as a gate to prevent unintended movements. Our false positive rate was 1.3%, meaning that unintended reaches were detected only 1.3% of the time that the BCI was in use. Because our task consisted of many reaches with little rest in between successive reaches, we believe that the false positive rate would be even lower in naturalistic settings, when the user would spend more time at rest than in motion. Neural activity during resting periods would likely be very different from that during active periods, so that false positive detections would be very unlikely during

resting periods.

Optimizing our decoder for a low false positive rate came at the cost of its sensitivity. We only detected only 44% of intended reaches, and this rate should be much higher for a useful clinical BCI system. One route to increased sesnsitivity while maintaining a low false positive rate would be a more methodical feature selection process. Currently, our algorithm makes use of neural power sampled every 50 ms for 500 ms before each time point in the motion data. This is repeated for two sensorimotor electrodes and two frequency bands, the beta band and the gamma band. We believe that using additional electrodes and frequency bands could improve the performance of the decoder. We also suspect that not all of the sampled points will prove necessary to be included. However, since the magnitudes of the input features to our decoder appear to be higher when movements are initiated from rest, it is reasonable to assume that our classifier will be more sensitive in naturalistic settings than it was in this experiment, even without any changes in the features being used.

Analysis into why a nearest neighbor classifier outperformed other types of classifiers has not been performed, but the reason likely has to do with the ability of this method to account for the high degree of single-trial variance in the data. For example, if one input feature at a time point has a very unusual value, the data point will still likely be closer to neighbors of the correct class than the incorrect class in the high-dimensional feature space. This robustness to high variance could be important when working with neural data, since only

a small portion of the variability in the data is due to the task at hand.

We have high confidence that, with improvements, our reach onset decoder could eventually be used in a real ECoG-driven manipulator. The low false positive rate achieved in our study is promising from a practical standpoint, as unwanted motion could potentially be eliminated from BCI manipulator control. In activities of daily living, it is more often the case that reaches are initiated from rest than as part of a prolonged sequence, and we believe this will lead to an improvement in the performance of our decoder. Finally, we note that the rhythms observable with ECoG have correlates that are observable both in EEG and single-cell BCI's, so these modalities may be able to apply our results in the future.

Index

Bibliography

[1] Nicholas R. Anderson, Tim Blakely, Gerwin Schalk, Eric C. Leuthardt, and Daniel W. Moran. Electrocorticographic (ECoG) correlates of human arm movements. *Exp Brain Res*, 2012.

[2] Trent J. Bradberry, Rodolphe J. Gentili, and Jose L. Contreras-Vidal. Reconstructing three-dimensional hand movements from noninvasive electroencephalographic signals. *The Journal of Neuroscience*, 30(9):3432–3437, 2010.

[3] BrainLatam.com. Utah array, 2018. [Online; accessed April 27, 2018].

[4] John K. Chapin, Karen A. Moxon, Ronald S. Markowitz, and Miguel A. L. Nicolelis. Real-time control of a robot arm using simultaneously recorded neurons in the motor cortex. *Nature*, 2(7):664–670, 1999.

[5] Jennifer L Collinger, Brian Wodlinger, John E Downey, Wei Wang, Elizabeth C Tyler-Kabara, Douglas J Weber, Angus J C McMorland, Meel Velliste, Michael L Boninger, and Andrew B Schwartz. High-performance neuroprosthetic control by an individual with tetraplegia. *Lancet*, 381:557–564, 2013.

[6] Nathan E. Crone, Diana L. Miglioretti, Barry Gordon, and Ronald P. Lesser. Functional mapping of human sensorimotor cortex with electro-

corticographic spectral analysis: II. event-related synchronization in the gamma band. *Brain*, 121:2301–2315, 1998.

[7] Nathan E. Crone, Diana L. Miglioretti, Barry Gordon, Jeffrey M. Sieracki, Michael T. Wilson, Sumio Uematsu, and Ronald P. Lesser. Functional mapping of human sensorimotor cortex with electrocorticographic spectral analysis: I. alpha and beta event-related desynchronization. *Brain*, 121:2271–2299, 1998.

[8] Apostolos P. Georgopoulos, Andrew B. Schwartz, and Ronald E. Kettner. Neuronal population coding of movement direction. *Science*, 233(4771):1416–1419, 1986.

[9] Eun Jung Hwang and Richard A. Andersen. Brain control of movement execution onset using local field potentials in posterior parietal cortex. *The Journal of Neuroscience*, 29(45):14363–14370, 2009.

[10] Gareth James, Daniela Witten, Trevor Hastie, and Robert Tibshirani. An introduction to statistical learning with applications in R. 2013.

[11] Laboratory for Neural Computation and Cognition, Brown University. Eeg, 2015. [Online; accessed April 27, 2018].

[12] Kai J. Miller, Eric C. Leuthardt, Gerwin Schalk, Rajesh P. N. Rao, Nicholas R. Anderson, Daniel W. Moran, John W. Miller, and Jeffrey G. Ojemann. Spectral changes in cortical surface potentials during motor movement. *The Journal of Neuroscience*, 27(9):2424–2432, 2007.

[13] Yasuhiko Nakanishi, Takufumi Yanagisawa, Duk Shin, Ryohei Fukuma, Chao Chen, Hiroyuki Kambara, Natsue Yoshimura, Masayuki Hirata, Toshiki Yoshimine, and Yasuharu Koike. Prediction of three-dimensional arm trajectories based on ecog signals recorded from human sensorimotor cortex. *PLOS One*, 8(8), 2013.

[14] G. Pfurtscheller, B. Graimanna, J.E. Hugginsc, S.P. Levine, and L.A. Schuhe. Spatiotemporal patterns of beta desynchronization and gamma synchronization in corticographic data during self-paced movement. *Clinical Neurophysiology*, 114:1226–1236, 2003.

[15] Tobias Pistohl, Tonio Ball, Andreas Schulze-Bonhage, Ad Aertsen, and Carsten Mehring. Prediction of arm movement trajectories from ECoG-recordings in humans. *Journal of Neuroscience Methods*, 167:105–114, 2008.

[16] Supratim Ray, Nathan E. Crone, Ernst Niebur, Piotr J. Franaszczuk, and Steven S. Hsiao. Neural correlates of high-gamma oscillations (60 200 Hz) in macaque local field potentials and their potential implications in electrocorticography. *The Journal of Neuroscience*, 28:11526–11536, 2008.

[17] E. M. Schmidt, M. J. Bak, and J. S. McIntosh. Long-term chronic recording from cortical neurons. *Experimental Neurology*, 52:496–506, 2007.

[18] Edward M. Schmidt. Spectral changes in cortical surface potentials during motor movement. *Annals of Biomedical Engineering*, 8:339–349, 1980.

[19] Andrew B. Schwartz, X. Tracy Cui, Douglas J. Weber, and Daniel W. Moran. Brain-controlled interfaces: Review movement restoration with neural prosthetics. *Neuron*, 52:205–220, 2006.

[20] Wikipedia, the free encyclopedia. Electrocorticography, 2014. [Online; accessed April 27, 2018].

[21] Jonathan R. Wolpaw and Dennis J. McFarland. Control of a two-dimensional movement signal by a noninvasive braincomputer interface in humans. *PNAS*, 101(51):17849–17854, 2004.

[22] Yasuo Nagasaka Zenas C. Chao and Naotaka Fujii. Long-term asynchronous decoding of arm motion using electrocorticographic signals in monkeys. *Frontiers in Neuroengineering*, 3(3), 2010.

Vita

Patrick Marino received his Bachelor of Science degree in Physics in 2014 and his Bachelor of Science in Mechanical Engineering in 2015 from the University of Notre Dame. He began work towards a Master of Science in Mechanical Engineering from The University of Texas at Austin in 2015.

Permanent address: pmarino@utexas.edu

This thesis was typeset with LaTeX[†] by the author.

[†]LaTeX is a document preparation system developed by Leslie Lamport as a special version of Donald Knuth's TeX Program.